Escola de Camins

Escola Tècnica Superior d'Enginyeria de Camins, Canals i Ports

UPC BARCELONATECH

PROJECTE O TESINA D'ESPECIALITAT

Títol

Treating inextensibility constraints in hyperelastic materials using inequality level sets

Autor/a

Eric Miranda Neiva

Tutor/a

Antonio Rodríguez-Ferran

Departament

Matemàtica Aplicada III

Intensificació

Enginyeria Computacional

Data

20 de juny de 2014

TREATING INEXTENSIBILITY CONSTRAINTS IN HYPERELASTIC MATERIALS WITH INEQUALITY LEVEL SETS

Student: Eric Miranda Neiva *Advisor:* Antonio Rodriguez-Ferran

Abstract. **Elastomers** are viscoelastic polymers with low Young's modulus and high failure strain that are used in many civil engineering applications, including bridge bearings, seismic isolators for buildings and resilient rail wheels.

Their constitutive behaviour is characterized by a nonlinear stress-strain relation with an extensibility limit. This contrasts with materials that have instead a limit on the tensile stresses, such as mild steel.

This MSc thesis is concerned with the **numerical modeling** of elastomers. This involves dealing with a medium with two phases: a constrained region, where the particles have reached their maximum allowable deformation, and a free region, where the **inextensibility constraint** is still inactive.

Moreover, one can think of an interface splitting the two phases of the medium. If the focus is put in obtaining methods to locate and evolve such interface, then a two phase medium with a moving interface is considered.

From the mathematical point of view, this is a constrained minimization problem. One of the strategies to solve it is to turn the minimization problem into a shape equilibrium one. This approach has been successfully employed for an interface location problem in small strains and serves as the starting point of this work.

Thus, the main purpose of this thesis is to extend this formulation to a **large strains** interface locating and evolving scenario. A first analysis of the problem reveals two sources of **nonlinearity**: the inextensibility constraint and the kinematics in large strains.

A simple but thorough one-dimensional study of the problem is then developed to find methods to sort out both nonlinearities. Following this, explicit iterative schemes to locate and evolve one or multiple interfaces are straightforwardly obtained in 1D linear elasticity.

However, the same ideas applied to a simple St.Venant-Kirchhoff **hyperelasticity** model, evidences that even very simple 1D problems become rather complex and cannot be solved as directly and explicit as before.

Numerical examples are provided throughout this analysis and they are also useful to conclude that both locating and evolving the interface can be essentially seen as the same problem, but with different driving effects.

After that, an extension of the one-dimensional schemes to two or more dimensions is explored. Although the same ideas can be applied, more sophisticated modeling tools are required, namely, the **X-FEM and Level set** methods, the **shape sensitivity** analysis and the **Arbitrary Lagrangian-Eulerian methods**.

A complementary numerical implementation of the proposed strategy is to show its computational benefits. In particular, a combination of the three previous techniques shall make unnecessary a stepwise update of the Level set.

The work presented here may not be limited to this particular case and be relevant to other engineering problems involving **moving interfaces and boundaries**, such as plasticity analysis or the saturation of a porous medium.

Keywords: Elastomer, numerical modeling, inextensibility constraint, large strains, nonlinearity, hyperelasticity, X-FEM and Level set, shape sensitivity, Arbitrary Lagrangian-Eulerian methods, moving interfaces and boundaries.

Wer mit Ungeheuern kämpft, mag zusehn,
dass er nicht dabei zum Ungeheuer wird.
Und wenn du lange in einen Abgrund blickst,
blickt der Abgrund auch in dich hinein.

— Friedrich Nietzsche, *Jenseits von Gut und Böse*.

ACKNOWLEDGMENTS

I would like to express my most sincere gratitude to all the people who have helped me in the course of this MSc thesis:

Antonio Rodriguez-Ferran, my advisor, for his constant availability, generous dedication and proper guidance; Prof. Nicolas Möes for the time he devoted discussing this thesis; Leire Asua, Irene Litago and Ana López for their readiness to help and moral support; Jorge Cañardo for the advice regarding the typesetting and all my friends at the FME who encouraged me to contact Antonio.

CONTENTS

LIST OF FIGURES

LIST OF TABLES

LIST OF SYMBOLS

$[\![\cdot]\!]$	Jump operator
α	Extensibility limit of the material
β	Scalar function, time depending component of the load
χ_A	The characteristic function of $A \subset \Omega$
Γ_d	Region of $\partial\Omega$ where a Dirichlet condition applies
Γ_n	Region of $\partial\Omega$ where a Neumann condition applies

$\hat{\mathbf{v}}$	Mesh velocity
$\hat{t}$	Neumann boundary condition at $x = L$
$\hat{u}$	Dirichlet boundary condition at $x = L$
λ	Lamé's first parameter
$\mathbb{C}$	Fourth-order stiffness or elasticity tensor
$\mathbb{U}$	Total potential energy of the system
$\mathbf{b}$	Body force vector per unit volume
$\mathbf{c}$	Convective velocity
$\mathbf{E}$	Second-order Green-Lagrange deformation tensor
$\mathbf{e}$	Second-order Euler-Almansi deformation tensor
$\mathbf{F}$	Second-order deformation gradient tensor
$\mathbf{S}$	Second-order second Piola-Kirchhoff stress tensor
$\mathbf{t}_n$	Vector of tractions prescribed at Γ_n
$\mathbf{u}_d$	Vector of displacements prescribed at Γ_d
$\mathbf{v}$	Material velocity
$\mathbf{v}_\Gamma$	Outward normal velocity of the interface
$\mathbf{w}$	Particle velocity as seen from the referential domain
$\mathbf{X}$	Material or Lagrangian coordinates
$\mathbf{x}$	Spatial or Eulerian coordinates
$\mathbf{x}^\tau$	Transformed coordinates in shape sensitivity analysis
f	Physical quantity
J	Determinant of the deformation gradient tensor
M	Mass component of an ODE or a DAE
p	Lagrange multiplier
x^*	Interface point in the deformed configuration
μ	Lamé's second parameter (the shear modulus)
∇^s	Symmetric gradient operator

Ω	An open domain in $\mathbb{R}^2$
Ω^0	Reference or initial configuration
Ω^τ	Transformed domain in shape sensitivity analysis
Ω^t	Current or deformed configuration
Ω_c	Constrained zone of Ω
Ω_f	Free zone of Ω
Ω_R^t	Referential configuration in the ALE kinematical description
ϕ	Level set function
$\boldsymbol{\chi}$	Reference coordinates in the ALE kinematical description
$\boldsymbol{\sigma}$	Second-order Cauchy stress tensor
$\boldsymbol{\varepsilon}$	Second-order small strains tensor
$\boldsymbol{\varphi}$	Equation of motion
b_0	Scalar function, spatial depending component of the load
c	Scalar function, integration of b in $[x, L]$
c_0	Spatial depending component of function c
E	Elastic or Young's modulus of the material
f	Right hand function of an ODE or a DAE
L	Length of the 1D truss
l	Length of the 1D truss in the deformed configuration
r	Residual tension function
t_c	Critical time (see Section 2.3)
x^*	Interface point in 1D linear elasticity (see Chapter 2)
$x^\pm$	Pair of interface points (see Section 2.4)
x_0	Initial approximation of the interface point x^*

This document uses normal fonts for scalar quantities a, lower case bold fonts for first-order tensors (vectors), upper case bold fonts for second-order tensors (matrices) $\mathbf{A}$ and fourth-order tensors for blackboard bold fonts $\mathbb{A}$.

Exceptions to this rule are the notation of the different coordinate systems and the classical notation for the stress and deformation tensors.

For instance, $\mathbf{X}$ refers to the coordinates in the material configuration, whereas $\mathbf{x}$ designates the coordinates in the spatial configuration, or $\mathbf{E}$ refers to the Green-Lagrange second-order tensor, but $\mathbf{e}$ to the Euler-Almansi second-order tensor.

Part I

TREATING INEXTENSIBILITY CONSTRAINTS IN HYPERELASTIC MATERIALS WITH INEQUALITY LEVEL SETS

1

A MEDIUM SUBJECT TO AN INEXTENSIBILITY CONSTRAINT

The first chapter of this work describes briefly the technological motivation and the precedents of the mechanical problem. After that, the main purposes and the analysis procedure are described. Finally, a reference statement of the problem is provided for the subsequent particularizations.

1.1 INTRODUCTION AND PURPOSES

Elastomers are viscoelastic polymers with low Young's modulus and high failure strain compared with other materials, Cowie [4]. For this reason, they have been widely employed in several civil engineering areas.

In seismic engineering, for instance, they are the main component of the base isolation bearings. These systems provide a superstructure the means to accommodate large lateral shear movements during earthquakes, see Figure 1.

This MSc thesis seeks to contribute to the numerical modeling of these kind of materials. Therefore, it is appropriate to start out by giving an overview of their nature.

The microstructure of elastomers at an unstrained state consists in randomly arranged finite molecular strands. The strands

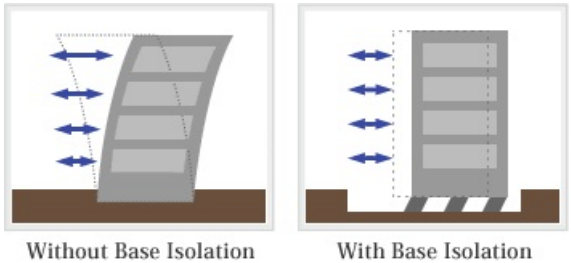

Figure 1: Seismic isolation in a building, from Nomura Research Institute.

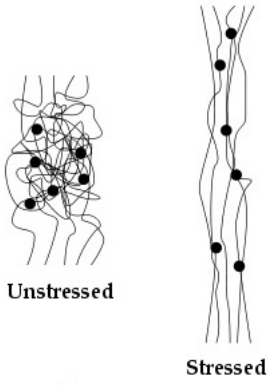

Figure 2: Molecular strands of an elastomer at unstressed and stressed states (dots represent the crosslinks). Adapted from the article *Elastomer* in Wikipedia.

defform affinely until some of them become fully stretched, as it is shown in Figure 2. Therefore, these materials are said to have a limit on its extensibility Gent [7].

In Figure 3 typical stress-strain curves for a ductile material, e.g. mild steel, and for rubber are shown. One can notice that, where the first has a limit on the tensile stress and softens with deformation, the second has a limit on the strains and hardens with deformation.

Following this example, one concludes that a rubber elasticity model at large strains must include a limiting value of at least one of the strain invariants [7].

The choice of the appropriate strain invariants and limiting values is not on the scope of this thesis, the focus is instead on

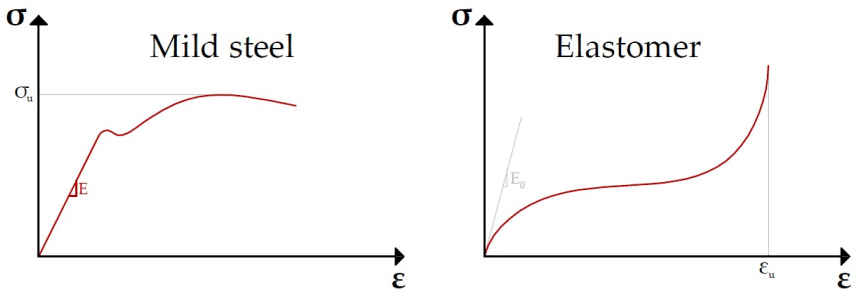

Figure 3: Stress-strain curves of mild steel and rubber compared

the numerical treatment of a continuum medium subject to an inextensibility constraint[1].

Among the approaches used to solve this engineering problem, two variants are considered. On the one hand, the classical approach turns the constrained minimization problem associated to the variational formulation into a saddle point problem using the Lagrange multiplier method.

On the other hand, a recently developed approach by Bonfils et al. [3] for a small strains interface location problem transforms the minimization problem into a shape equilibrium one using a Level set and X-FEM strategy.

Motivated by better rates of convergence and numerical stability, the work presented here will essentially revolve around this second approach. In particular, the main purpose is to take the formulation presented in [3] and extend it to a finite strain setting, since it is the scenario where an extensibility limit for an elastomer has full sense.

In parallel with this, it is aimed to add duly modifications to the method in order to obtain the most explicit possible way to describe the interface. Regardless of the numerical stability, a more explicit method will provide a computational benefit. The effects of applying a variable load will also be incorporated.

The main tools which support this work include the elasticity theory for small and large strains of the continuum mechanics, Oliver and Agelet [13]; and basic concepts of constrained optimization, Nocedal and Wright [12] and numerical methods for ordinary and partial differential equations, Lambert [9] and Quarteroni [15].

A one-dimensional linear elastic problem is considered as the starting point of the analysis. In this ground scenario, the idea of enforcing the inequality constraint within a continuum medium is clearly shown.

Iterative schemes considering different boundary conditions to locate and evolve the interface are obtained and they are re-

1 An extensibility constraint limits the deformation of a body, thus it can be alternatively called a kinematic constraint.

markable for its explicitness.

The study continues with the one-dimensional extension to a hyperelastic setting. There it is shown how very simple one-dimensional problems acquire a complexity that challenges the possibility of tracking the interface as directly as in the previous case.

Throughout the discussion, we will identify sources of nonlinearity, show numerical examples depicting such behaviour and analyse how to deal with them.

The last part of the work intends to link the strategies and conclusions of the 1D analysis to a 2D or a 3D scenario. In particular, we address the possible modifications and extensions of the approach given in [3].

1.2 STATEMENT OF THE PROBLEM

Several definitions of the mechanical problem are considered in this study, depending on body dimension, elasticity framework and boundary conditions.

Nonetheless, it is more practical to establish a reference statement of the problem and understand the subsequent formulations as derivations from the original one.

For this purpose, let us choose a linear elasticity 2D interface location problem. After that, the necessary large strain elasticity tensors are defined to introduce the extension of the model to large strains.

This chapter contains the first identification of the particularities associated to modeling a medium subject to an inextensibility constraint.

1.2.1 *The 2-dimensional linear elastic model*

Let us consider an open two-dimensional domain denoted by Ω, as shown in Figure 4. On the boundary Γ_d a Dirichlet condition $\mathbf{u} = \mathbf{u}_d$ is prescribed, whereas on the boundary Γ_n a Neumann condition $\mathbf{t} = \mathbf{t}_n$ is imposed. An external body force $\mathbf{b}$ acts over the whole domain.

Following Bonfils et al. [3], one can think of an interface Γ splitting the domain into two disjoint regions: the constrained zone Ω_c, where the extensibility constraint is active, and the free or inactive zone Ω_f.

Note that the body is now assumed to be a two-phase elastic medium and that the interface is not known a priori.

A volumetric constraint of the form

$$\operatorname{tr}(\boldsymbol{\varepsilon}) - \alpha \leqslant 0, \tag{1.1}$$

where $\alpha > 0$ is the extensibility limit, is adopted to model the inextensibility of the material.

Based on the theory of linear elasticity and introducing a Lagrange multiplier p to incorporate this constraint, the strong

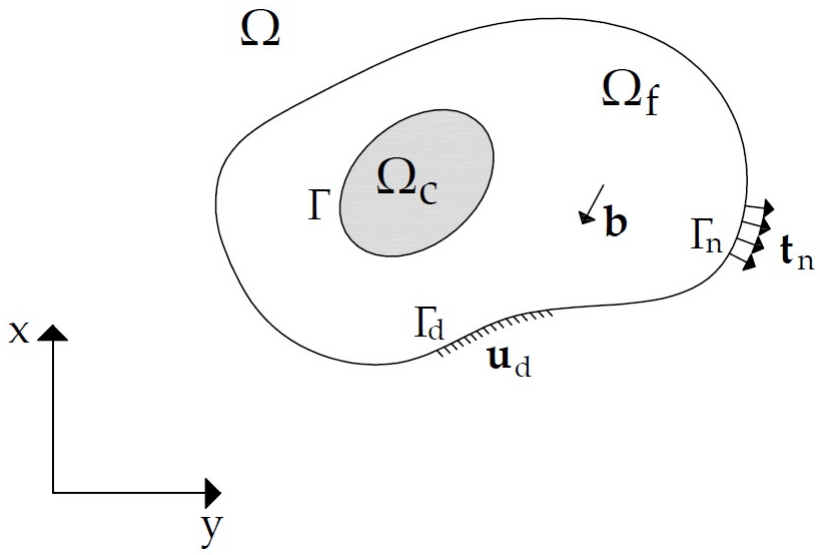

Figure 4: The 2D linear elastic model. Adapted from Bonfils et al. [3].

form[2] of the problem reads as in Table 1.

Regarding the conditions on the interface Γ, no separation, no slip and no penetration of Ω_c and Ω_f may occur, see Figure 5. This is achieved by imposing continuity of displacements along Γ.

On the other hand, continuity of tractions along Γ needs also be verified, otherwise equilibrium on the whole domain does not hold. Thus, $[\![\cdot]\!]$ in Table 1 denotes the jump operator.

2 The variational formulation is left at Appendix A, as it is not required for the 1D analysis.

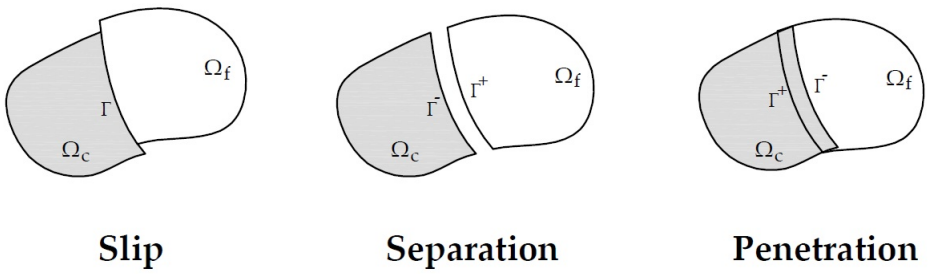

Figure 5: Slip, separation and penetration of an interface.

Nonetheless, the earlier jump conditions do not assure strain continuity along Γ; indeed, a discontinuity holds along the interface and needs to be modeled accordingly, see Section 4.1.

As the Lagrange multiplier p is introduced in the strong form, the solution of the problem must verify the Karush-Kuhn-Tucker optimality conditions provided in Table 1.

Observation of the statement yields the first relevant remark. Although the chosen kinematics are linear, the presence of the restriction sets a source of non-linearity in the problem. Chapter 2 deals with this matter and shows numerical examples of this behaviour.

1.2.2 *Extension to a St.Venant-Kirchhoff model*

The large strain tensors[3] that will be used in the subsequent chapters are defined in this section. Addition of superscripts to the domain notation, namely Ω^0 and Ω^t, indicates the reference or initial and current or deformed configurations, respectively.

The deformation gradient tensor $\mathbf{F}$ reads

$$\mathbf{F} = \frac{\partial \mathbf{x}}{\partial \mathbf{X}} \qquad F_{ij} = \frac{\partial x_i}{\partial X_j} \qquad i,j = 1,2, \tag{1.2}$$

where $\mathbf{X} \in \Omega^0$ and $\mathbf{x} \in \Omega^t$ refer to the Lagrangian or material coordinates and the Eulerian or spatial coordinates, respectively, see Figure 6.

Furthermore, the determinant of the deformation gradient tensor is denoted by J.

On the other hand, the relation between the spatial Cauchy stress tensor $\boldsymbol{\sigma}$ and the material second Piola-Kirchhoff stress tensor $\mathbf{S}$ is given by

$$\boldsymbol{\sigma} = J^{-1}\mathbf{F}\mathbf{S}\mathbf{F}^T \qquad \sigma_{ij} = J^{-1}F_{ik}S_{kl}F_{jl} \qquad i,j,k,l = 1,2. \tag{1.3}$$

Regarding the deformation quantities, the Euler-Almansi or spatial deformation tensor reads

$$\mathbf{e}(\mathbf{x},t) = \frac{1}{2}(\mathbf{Id} - \mathbf{F}^{-T}\mathbf{F}^{-1}) \quad e_{ij}(\mathbf{x},t) = \frac{1}{2}(\delta_{ij} - F^{-1}_{ki}F^{-1}_{kj}) \quad i,j,k = 1,2,$$

3 Some notes on tensor calculus are given in Spivak [16].

(1.4)

whereas the Green-Lagrange or material deformation tensor has the form

$$\mathbf{E}(\mathbf{X},t) = \frac{1}{2}(\mathbf{F}^T\mathbf{F} - \mathbf{Id}) \quad E_{ij}(\mathbf{x},t) = \frac{1}{2}(F_{ki}F_{kj} - \delta_{ij}) \quad i,j,k = 1,2. \tag{1.5}$$

In the spirit of limiting the study to identifying and dealing with the numerical challenges of an extension to large strains, a simple model of a St.Venant-Kirchhoff hyperelastic[4] material is chosen, whose isotropic constitutive relation reads

$$\mathbf{S} = \lambda tr(\mathbf{E})\mathbf{Id} + 2\mu E. \tag{1.6}$$

The finite strain version of Table 1 can be obtained using the previous definitions and Equation 1.6, but this will not be detailed here. The discussion will instead be driven towards the second main source of non-linearity in this study, namely, the non-linear kynematics.

4 A good definition is found at chapter 6 of Bonet and Wood [2]: A hyperelastic material is an elastic material with a path-independent behaviour. Consequently, a stored strain energy function or elastic potential per unit volume can be defined as the work done by the stresses from the initial to the current configuration.

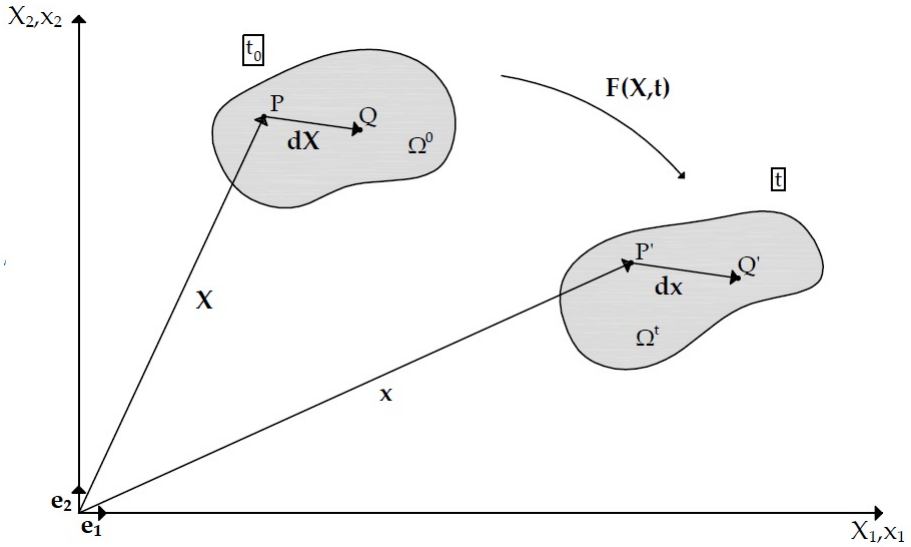

Figure 6: Description of motion in 2D finite deformation. Adapted from Oliver and Agelet [13].

It is widely known that, in the more general framework of large strains, displacements and displacement gradients are not necessarily small. Thus, material and spatial descriptions do not coincide, as it happens in small strains elasticity.

Mechanical equilibrium, on the other hand, is applied on the deformed or current configuration. For instance, the finite strain version of the translational equilibrium equation, see Bonet and Wood [2], written in Table 1 reads in its integral form

$$\int_{\partial\Omega^t} \boldsymbol{\sigma}\mathbf{n}\,da + \int_{\Omega^t} \mathbf{b}\,dv = 0. \tag{1.7}$$

Both Equation 1.6 and Equation 1.7 are non-linear. In contrast with the linear elastic model, the hyperelastic model contains two sources of nonlinearity: extensibility constraint and kinematics. Chapter 3 shows how both phenomena can be treated.

	Ω_c	Γ	Ω_f
Mechanical equilibrium	$\mathrm{div}\boldsymbol{\sigma} + \mathbf{b} = \mathbf{0}$		$\mathrm{div}\boldsymbol{\sigma} + \mathbf{b} = \mathbf{0}$
Constitutive relation	$\boldsymbol{\sigma} = \mathbb{C} : \boldsymbol{\varepsilon} + p\mathbf{Id}$		$\boldsymbol{\sigma} = \mathbb{C} : \boldsymbol{\varepsilon}$
Kinematic conditions	$\boldsymbol{\varepsilon} = \nabla^s \mathbf{u}$		$\boldsymbol{\varepsilon} = \nabla^s \mathbf{u}$
Boundary conditions	$\boldsymbol{\sigma}\mathbf{n} = \mathbf{t}_n$ on $\partial\Omega_c \cap \Gamma_n$	$[\![\boldsymbol{\sigma}\mathbf{n}]\!] = \mathbf{0}$	$\boldsymbol{\sigma}\mathbf{n} = \mathbf{t}_n$ on $\partial\Omega_f \cap \Gamma_n$
	$\mathbf{u} = \mathbf{u}_d$ on $\partial\Omega_c \cap \Gamma_d$	$[\![\mathbf{u}]\!] = \mathbf{0}$	$\mathbf{u} = \mathbf{u}_d$ on $\partial\Omega_f \cap \Gamma_d$
Optimality conditions	$\mathrm{tr}(\boldsymbol{\varepsilon}) - \alpha = 0$	$\mathrm{tr}(\boldsymbol{\varepsilon}) - \alpha = 0$	$\mathrm{tr}(\boldsymbol{\varepsilon}) - \alpha \leqslant 0$
	$p \leqslant 0$	$p = 0$	$p = 0$

Table 1: Strong form of the 2D linear elastic problem.

2

AN INEXTENSIBILITY CONSTRAINT IN 1D LINEAR ELASTICITY

A 1D small strains model with an extensibility limit is the chosen problem to start this analysis. Following the assumption of basic hypotheses, numerical schemes to locate and displace the interface are developed in a rather straightforward way.

2.1 PRELIMINARY HYPOTHESES

Recalling Section 1.2.1, let us consider a 1D truss of length L subject to a prescribed load, see Figure 7, represented by a piecewise continuous function $b\colon [0, L] \to \mathbb{R},\ b \geqslant 0$. Note that interest in extension behaviour accounts for positiveness of b.

The extensibility constraint reads in this case

$$\alpha > 0,\ \varepsilon(x) \leqslant \alpha,\ 0 \leqslant x \leqslant L. \tag{2.1}$$

Furthermore, the fourth-order stiffness tensor reduces to the Elastic or Young's modulus E and the interface to a point x^* in the segment $[0, L]$. In contrast with the 2D setting, continuity of tractions accounts for continuity of strains at x^*.

The analytical solution considering a bar fixed at its left edge is provided at Appendix B. There it is shown that the the Lagrange multiplier admits a practical interpretation independent on the boundary condition at the right edge of the bar:

$$p(x) = \langle \sigma(x) - E\alpha \rangle. \tag{2.2}$$

Figure 8 compares the plots of the analytical solution for two constant loading cases and shows evidence of non-linearity due

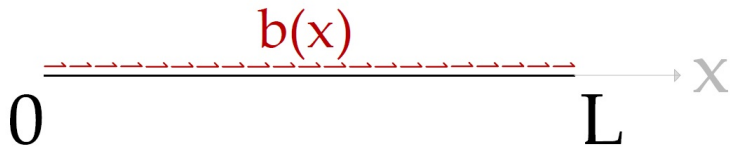

Figure 7: 1D truss subject to a prescribed tensile load.

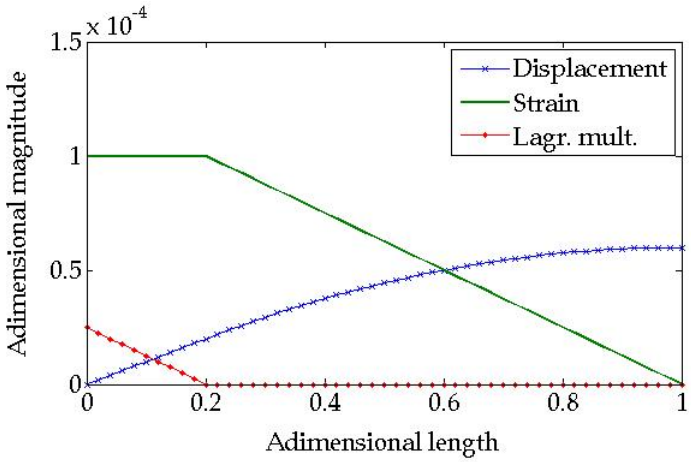

(a) $b(x) \equiv 1.25 \cdot 10^{-4}$ and $\alpha = 1.0 \cdot 10^{-4}$

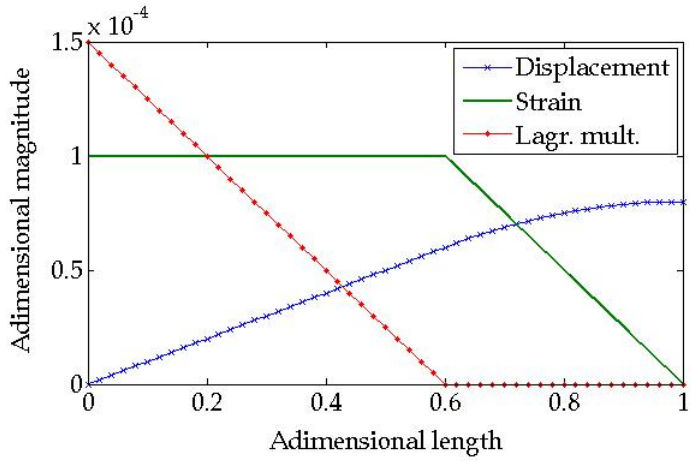

(b) $b(x)/E \equiv 2.5 \cdot 10^{-4}$ and $\alpha = 1.0 \cdot 10^{-4}$

Figure 8: Analytical solution for constant load.

to the extensibility constraint. In spite of doubling the load, the second interface does not locate at two times the position of the first interface. Alternatively, one may state that the superposition principle does not hold.

2.2 LOCATING THE INTERFACE

The subject of interest is now put in devising a Newton-Raphson scheme to locate the interface x^* for a 1D linear elastic problem complying with the criterion given in Section 2.1.

Inspired by Equation 2.2, one aims to find $x^* \in [0, L]$ such that the Lagrange multiplier cancels out. For instance, by taking Figure 8a and incorrectly locating the interface, one sees that $p(x^*) \neq 0$, see Figure 9.

This leads to the definition of the *residual tension* function as

$$r(x) := \sigma(x) - E\alpha, \quad x \in [0, L], \tag{2.3}$$

and, consequently, the root-finding problem reads in abstract form

$$\text{find } x^* \in [0, L] \text{ such that } r(x^*) = 0, \tag{2.4}$$

which will be developed considering the following boundary conditions at the tip of the truss:

A. $\sigma(L) \equiv \hat{t}$, Neumann boundary condition at $x = L$.

B. $u(L) \equiv \hat{u}$, Dirichlet boundary condition at $x = L$.

It is relevant to point out that, if the iterative scheme converges, then the solution must be the interface x^*; indeed, if

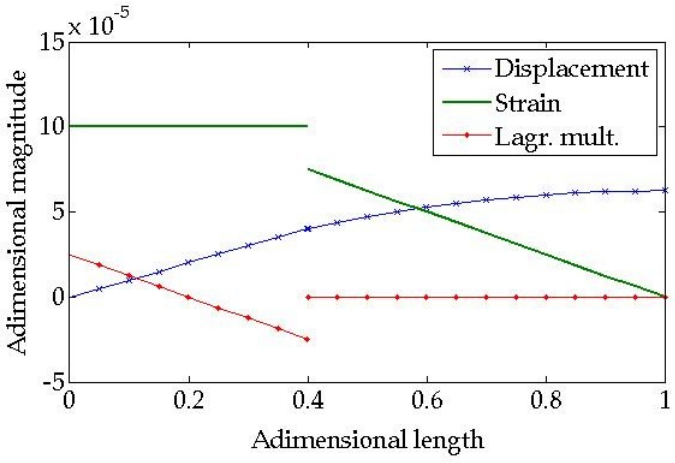

Figure 9: 1D solution for an incorrectly located interface.

LOCATING THE INTERFACE IN 1D LINEAR ELASTICITY. NEWTON-RAPHSON METHOD

Given $x^0 = x_0 \in [0, L]$ an initial approximation,

for $k > 0$, find x^{k+1} such that $\quad x^{k+1} = x^k + \dfrac{\hat{t} + c(x^k) - E\alpha}{b(x^k)}$

Table 2: Interface localization in 1D linear elasticity.

there exists a x^* in $[0, L]$ that satisfies Equation 2.4, then it must be unique according to Rolle's theorem. Otherwise, b must vanish at some point in $[0, L]$ and this contradicts the hypothesis of positiveness.

It suffices to use the integral form of the equilibrium equation in $[x, L]$ to evaluate the residual stresses $r(x)$ at a given point and also, after derivation, to find the direction at each step.

The explicit form of Equation 2.4 is written in Table 2, accompanied by the describing Figure 10.

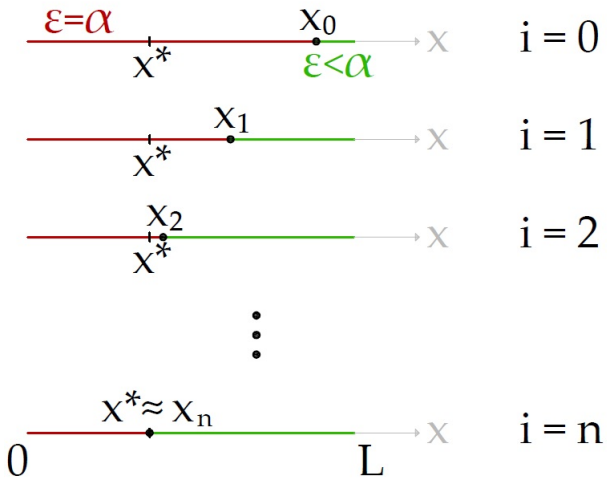

Figure 10: Description of the 1D location scheme.

Note that $c\colon [0, L] \to \mathbb{R}$ is given by

$$c(x) := \int_x^L b(s)ds. \tag{2.5}$$

If a Dirichlet boundary condition holds, then the stresses at L are obtained via the kinematic condition. Thus,

$$\hat{t}(x) = \frac{E}{L-x}\left[\hat{u} - \alpha x - \frac{1}{E}\int_0^{L-x}\left[\int_t^{L-x} b(s+x)ds\right]dt\right]. \tag{2.6}$$

In physical terms, a Neumann boundary condition yiels the analysis of a bar fixed at its left edge (isostatic), whereas a Dirichlet boundary condition a bar fixed at both edges (hyperstatic). Thus, a suitable compatibility condition is required for the second case.

Mathematically, this results from the fact that fixing the derivative of the function at a given point (Neumann) is a stronger condition than fixing the value of the function (Dirichlet) at a given point.

2.2.1 *Numerical approach*

Let us now proceed with some details about the numerical implementation of Equation 2.4.

Regarding the treatment of the integral terms involved in the numerical scheme, they will be computed using a Gaussian

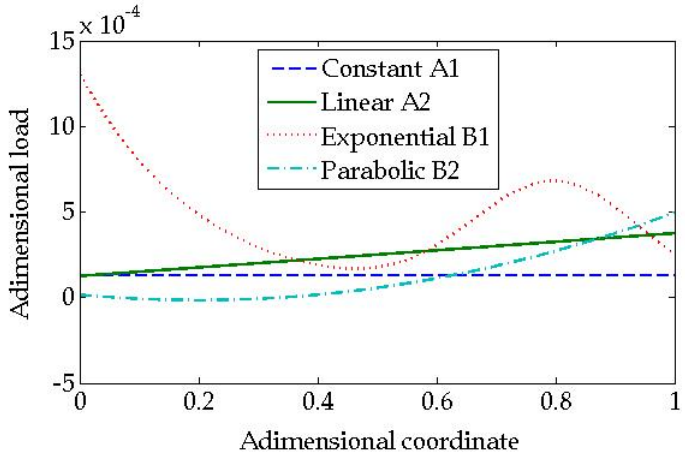

Figure 11: Selection of loading cases.

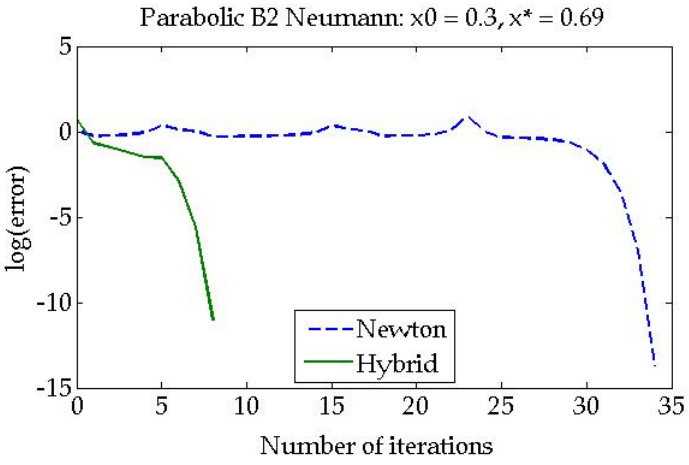

Figure 12: Improvement in convergence rates.

quadrature. The fact that b is known along the segment $[0, L]$ and the high accuracy of these methods account for this decision.

It is widely known that the Newton-Raphson procedure is locally convergent. One may combine the Bisection method with the Newton method, when convergence of the second fails or has an abnormal low rate. This strategy is the so called Hybrid method.

Figure 11 depicts a selection of load functions with the aim of testing the numerical performance of the implementation. For these load cases, Figure 12 shows a comparative example.

2.3 EVOLVING THE INTERFACE

Recovering Section 2.1, additional hypotheses are required to model a variable load responsible for the displacement of the interface.

For this purpose, let us assume that the prescribed load can be written as $b(x,t) = \beta(t)b_0(x)$, where $\beta\colon [0,\infty) \to \mathbb{R}$, $\beta(0) = 0$, is monotonically increasing and $b_0\colon [0,L] \to \mathbb{R}$, $b_0(x) \neq 0\ \forall x \in [0,L]$, are both continuous.

As a result of considering a quasistatic process, that is, of neglecting dynamic effects, variable t cannot be interpreted as the physical time, but as a pseudotime o ficticious time.

Thus, variable t serves the sole purpose of representing a variable load and, in particular, the progressive application of an external load.

Nonetheless, a quasistatic process does not influence the analysis presented below. It is true that magnitudes such as velocity of the interface will not have any physical sense here, but the path of the interface does not depend on load velocity application.

After this remark, the obtention of numerical schemes to describe the evolution of the interface can be introduced. Recalling Section 2.2 appropriate transformations of the equilibrium equation (plus the kinematic condition for the Dirichlet case) and derivation in the ficticious time t result in ODEs of the form

$$M(t,x^*)\,\dot{x}^* = f(t,x^*); \quad x^*(t) \in [0,1], \ \ \forall t \in [t_c,\infty). \tag{2.7}$$

According to the hypothesis on β, Equation 2.7 holds only for $t \in [t_c,\infty)$, where $t_c \geqslant 0$, the *critical time*, is the value of t that verifies $x^*(t) = 0$.

In other words, at t_c the nucleation of a restricted zone takes place, that is, one point in the bar reaches the extensibility limit.

Table 3 summarizes the ODEs obtained for each boundary condition defined in Section 2.2, see also Figure 13. Detailed

explanation of how they are reached is left at Appendix C.

Concerning the critical time, t_c is the solution of

$$E\alpha - \hat{t} - \beta(t)\int_0^L b_0(s)ds = 0, \tag{2.8}$$

for the Neumann case, whereas for the Dirichlet case the equation reads

$$E\alpha - \beta(t)\int_0^L \left[b_0(s) - \frac{1}{L}\int_s^L b_0(q)dq\right] ds = 0. \tag{2.9}$$

Refer to Appendix D for a simple example of the *critical time* concept. There, it is additionally shown that mass scalar M is zero for $(t_c, x^*(t_c))$ in the Dirichlet case.

When the mass component of a differential equation has singular values, then usage of the term DAE (differential algebraic equation, Hairer and Wanner [8]) is more appropriate than ODE. Section 2.4 devises a strategy to overcome this numerical challenge.

	NEUMANN B.C.	DIRICHLET B.C.
$M(t, x^*)$	$\beta(t)b_0(x^*(t))$	$\beta(t)(L - x^*(t))b_0(x^*(t))$
$f(t, x^*)$	$\dot{\beta}(t)c_0(x^*(t))$	$\dot{\beta}(t)\int_{x^*(t)}^L \left(\int_{x^*}^x b_0(s)ds\right) dx$

Table 3: Description of the terms involved in Equation 2.7.

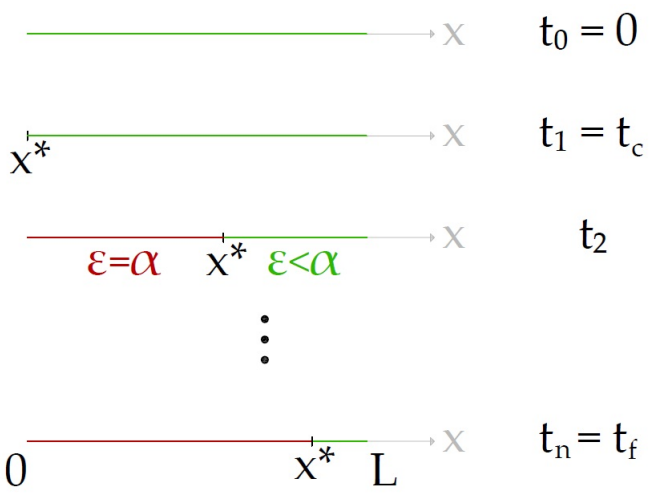

Figure 13: Description of the 1D evolution scheme.

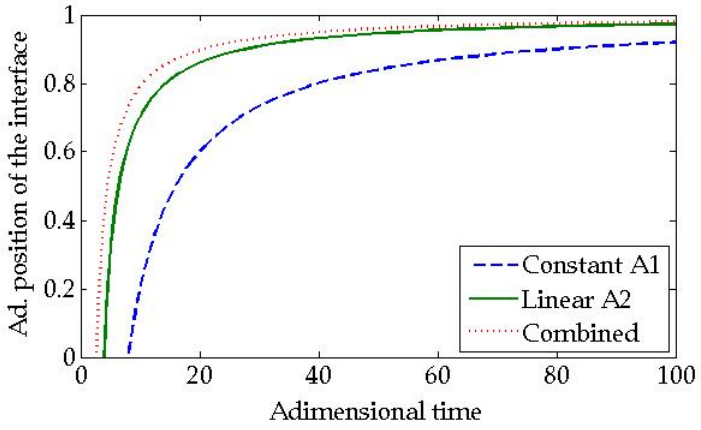

Figure 14: Evolution of the interface for different loading cases.

Observation of Table 3 and the above expressions allows to state that, in 1D linear elasticity, one only needs to know the geometry of the 1D truss and the external load to explicitely describe the evolution of the interface.

The same applies to the location schemes developed in Section 2.2. In conclusion, intrinsic non-linearity of the inextensibility problem can be easily treated in 1D linear elasticity and poses very few restrictions.

2.3.1 *Numerical approach*

Numerical implementation of Equation 2.7 is straightforwardly done with an explicit method to solve Ordinary Differential Equations such as the Runge Kutta Dormand-Prince, see Dormand and Prince [6], the default method in MATLAB and GNU Octave's *ode45* solver.

Apart from recapturing the non-linearity of the problem in the combined case, Figure 14 displays the hyperbolic evolution of the interface for a Neumann case.

In physical terms, it is natural to think of the fully constrained scenario as a limit case. Thus, incremental displacement of the interface is to decrease with the progressive application of the load.

2.4 DEALING WITH MULTIPLE INTERFACES

The aim of this section is to extend the evolution schemes to model external loads that create multiple interfaces. The analysis is restricted to a two interface scenario, but guidelines for three and more interface scenarios are provided.

Let us first modify the current assumptions in the following way: The prescribed load b is similarly decomposed, but b_0 has exactly one root $\forall x \in [0, L]$. Thus, a parabolic law of deformation is expected and for all $t > t_c$ there exists at most two $x^* \in [0, L]$ interfaces[1], namely, $x^-(t)$ and $x^+(t)$.

If multiple interfaces appear, then the earlier defined ODEs become the system of differential equations

$$\mathbf{M}(t, \mathbf{x}^*)\ \dot{\mathbf{x}}^* = \mathbf{f}(t, \mathbf{x}^*), \tag{2.10}$$

where $\mathbf{x}^*(t) = [x^-(t), x^+(t)]^t \in [0, 1]$ and $t \in [t_c, \infty)$.

As expected, a *critical time* also applies. It is clear that the nucleation happens at t_c and must coincide with the local maximum of the law of deformation, but derivation of the equilibrium equation proves that this point is the only root of b.

Therefore, mass matrix $\mathbf{M}$ is strictly singular for $(t_c, x^*(t_c))$ and Equation 2.10 is a system of DAEs. This phenomenon slightly complicates the numerical approach of the problem, as it is discussed in the subsequent numerical examples.

Concerning the Neumann case, given the fact that the equilibrium equation holds locally, it suffices to repeat the procedure in Section 2.3 for each interface.

Table 4 contains the resulting system of DAEs, where it is evident that the evolution of the two interfaces can be described separately, more precisely, the system of DAEs differs only in the initial condition.

As for the Dirichlet case, the equilibrium equations in $[x^{\pm}, L]$ and the kinematic condition (compatibility equation) are gathered and a system of 3 equations, whose 3 unknowns are $x^{\pm}$

1 The structure of the constrained and the free zones depend on the loading case.

and $\sigma(L,t)$, is obtained.

Derivation of these equations provides the system of DAEs that reads in Table 4. In contrast with the Neumann case, the evolution of the interfaces does not only differ in the initial condition, but it is still decoupled.

Based on this discussion, it is not difficult to see how these numerical schemes can be extended to the arbitrary n interfaces problem.

On the one hand, the Neumann DAEs system may be obtained after deriving the n equilibrium equations corresponding to the n interfaces, whereas the Dirichlet DAEs system also requires the compatibility equation.

2.4.1 *Numerical approach*

Let us construct now a simple example in order to illustrate the numerical challenges of Equation 2.10 and how to deal with them.

Suppose a Neumann problem given by a linear antisymmetric steady load $b_0(x) = b_0 x$, $\forall x \in [-L/2, L/2]$ (coordinates displaced for convenience) and a linear time factor: $\beta(t) = t$, $\forall t \in$

	NEUMANN B.C.
$\mathbf{M}(t,\mathbf{x}^*)$	$\beta(t)\begin{pmatrix} b_0(x^-(t)) & 0 \\ 0 & b_0(x^+(t)) \end{pmatrix}$
$\mathbf{f}(t,\mathbf{x}^*)$	$\dot\beta(t)\begin{pmatrix} c_0(x^-(t)) \\ c_0(x^+(t)) \end{pmatrix}$
	DIRICHLET B.C.
$\mathbf{M}(t,\mathbf{x}^*)$	$\beta(t)\begin{pmatrix} -x^-(t)b_0(x^-(t)) & 0 \\ 0 & (L-x^+(t))b_0(x^+(t)) \end{pmatrix}$
$\mathbf{f}(t,\mathbf{x}^*)$	$\dot\beta(t)\begin{pmatrix} \int_0^{x^-(t)}\left(\int_x^{x^-(t)} b_0(s)ds\right)dx \\ \int_{x^+(t)}^{L}\left(\int_{x^+(t)}^{x} b_0(s)ds\right)dx \end{pmatrix}$

Table 4: Description of the terms written in Equation 2.10.

$[0, \infty)$.

Application of Table 4 yields the system of DAEs $\forall\ [t_c, \infty)$:

$$\begin{aligned} \dot{x}^* &= \frac{-\frac{1}{2}\left(\frac{L^2}{4} - x^{*2}\right)}{t x^*}, \\ x^*(t_c) &= 0. \end{aligned} \tag{2.11}$$

Where the dependance on b_0 is implicitly within the initial condition for t_c.

One way to avoid the singularity at $t = t_c$ is to use a fully implicit numerical integration method. Thus, an evaluation of the function at $t = t_c$ is no longer required.

Putting this idea into practice with a backward Euler method produces the iterative scheme in Table 5. Interestingly, a fully implicit method provides here a major computational advantage compared with an explicit method.

If one aims to obtain maximum computational efficiency, then one possibility is to combine an explicit method and a fully implicit method, so that the second is only invoked at the nucleation singularity.

BACKWARD EULER METHOD FOR A SIMPLE TWO-INTERFACE CASE

Given $x^0 = 0$, *an initial approximation,*

for $k > o$, *find* x^{k+1} *such that* $\quad x^{k+1} = \dfrac{x^k \pm \sqrt{D^k}}{2 + \frac{\Delta t}{t_c + (k+1)\Delta t}}$,

where the discriminant reads:

$$D^k = (x^k)^2 + \frac{\Delta t L^2}{4(t_c + (k+1)\Delta t)}\left(2 + \frac{\Delta t}{t_c + (k+1)\Delta t}\right), \quad k \geqslant 0.$$

Table 5: Backward Euler method for multiple interfaces.

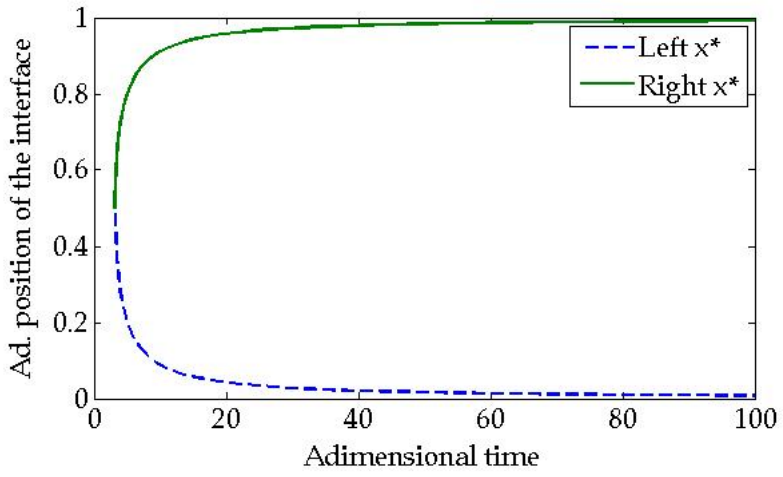

(a) Antisymmetric load

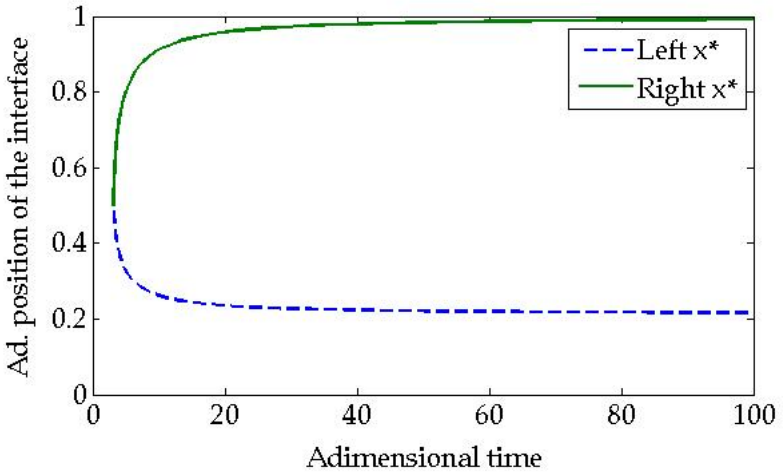

(b) Linear 1 to 3 load

Figure 15: Evolution of the interfaces for a linear centered load.

Figure 15 displays the graphical outcomes of applying this idea with a Neumann boundary condition, which can also be used to solve the numerical issues appearing in Section 2.3.

Note that the ratio between the ficticious time derivatives is easily found for this case:

$$\frac{\dot{x}^+(t)}{\dot{x}^-(t)} = \frac{c_0(x^+(t))b_0(x^+(t))}{c_0(x^-(t))b_0(x^-(t))} = \frac{b_0(x^+(t))}{b_0(x^-(t))}, \tag{2.12}$$

which allows to confront loading cases where the constrained zone evolves symmetrically with asymmetrically evolving cases.

3

AN EXTENSIBILITY CONSTRAINT IN 1D HYPERELASTICITY

On the basis of the previous chapter, it is aimed here to extend the developed numerical schemes to a large strains setting.

As a consequence of kinematic non-linearity, it will be seen that this is possible but for very particular cases.

3.1 PRELIMINARY ANALYSIS

The basic hypotheses given in Chapter 2 can be adapted using Section 1.2.2. Appendix E provides the numerical solution of the problem using two different approaches.

Following the discussion in Section 2.4, given the geometry of the truss and a load function, one can by means of the equilibrium equation (and the compatibility condition, if needed) obtain an explicit expression of $x^*(t)$ in small strains.

Inspired by this, Equation 3.1 provides the 1D traslational equilibrium in $[x^*(t), L]$ in the spatial or current configuration:

$$\sigma(L,t) - \sigma(x^*,t) + \int_0^{l(t)} b(x)dx = 0. \tag{3.1}$$

It is clear that $l(t)$, that is, the lenght of the deformed bar, is not known a priori.

One would immediately think that the material description is more suitable to locate and evolve the interface, but Equa-

Figure 16: 1D problem in large strains.

tion 3.2 shows that an additional unknown remains after applying the change of coordinates.

$$\sigma(L,t) - \sigma(X^*,t) + \int_0^L \mathbf{b}(X)\, J dX = 0 \tag{3.2}$$

Therefore, the effects of non-linear kinematics are evident: unless extra assumptions are made, there is no way to locate and evolve the interface without solving first the strong form of the problem.

The above statement, however, does not apply for the Eulerian description with a Dirichlet boundary condition. In this situation, $l(t)$ is known for all t in $[t_c, \infty)$ (e.g. $l(t) \equiv L$ for a Dirichlet homogeneous b.c.). From this point on, this is the case supposed for the numerical examples in this chapter.

Although determining the interface whether in the spatial configuration or in the material configuration is equivalent from the mathematical point of view, the interface of a continuum medium is not a set of particles, it is a set of points that separates the constrained and the free zones.

Thus, the physical sense of the interface is only preserved in the Eulerian spatial configuration and this is the description where it is more interesting to solve the problem.

Finally, in order to maintain consistency within the approach, the extensibility limit α is established on the spatial deformation tensor. In particular, the volumetric constraint reads

$$\mathrm{tr}(e) - \alpha \leqslant 0. \tag{3.3}$$

3.2 ADAPTING THE STRATEGIES FROM CHAPTER 2

Let us move now with devising schemes to treat the interface using the spatial description of a 1D truss with a Dirichlet homogeneous boundary condition.

Note that the focus is put on evolving schemes, because the method presented below is similarly applied to the locating schemes.

One way to overcome the additional complexity of non-linear kinematics in a St.Venant-Kirchhoff model could be to use algebraic manipulations of the tensors and the constitutive relation in Section 1.2.2 to obtain an equation, whose unknown could be whether e or $\frac{\partial u}{\partial x}$ and its coefficients dependant on $\sigma(x,t)$, known via Equation 3.1.

For instance, choosing e, one would end up obtaining a cubic equation which could be solved using Cardano's formulas, though the discussion of the roots would be quite an issue. Then, by imposing the boundary condition using

$$\int_0^{l(t)\equiv L} \frac{\partial u}{\partial x} dx = 0, \tag{3.4}$$

and derivating in t, one would get a large strains equivalent form of Equation 2.7.

However, this approach involves many arithmetic calculations (subtractions and divisions of numbers with different order of magnitude) and numerically it would be more convenient to avoid them for conditioning purposes.

Therefore, another approach is advised. Let us first give the spatial St.Venant-Kirchhoff constitutive relation, that is,

$$\sigma(x,t) = \frac{2\mu e(x,t)}{(1-2e(x,t))^{(3/2)}}. \tag{3.5}$$

And its plot in $e-\sigma$ adimensional coordinates in Figure 17.

It can be immediately seen that Equation 3.5 provides a one to one correspondance between e and σ, for $e \in [-1, 1/2]$[1]. That

1 Note that e is a deformation magnitude, thus values below -1 do not have any physical sense.

	DIRICHLET B.C. - SPATIAL DESCRIPTION
$M(t, x^*)$	$\beta(t) b_0(x^*) \int_{x^*}^{L} \frac{(1-2e(x,t))^2}{1+e(x,t)} dx$
$f(t, x^*)$	$\dot{\beta}(t) \int_{x^*}^{L} \frac{(1-2e(x,t))^2}{1+e(x,t)} \left(\int_{x^*}^{x} b_0(s) ds \right) dx$

Table 6: Terms involved in the large strains version of Equation 2.7.

means, a root-finding algorithm is well-defined to find $e(x, t)$ from $\sigma(x, t)$.

Apart from that, non-linearity of the correspondance accounts for the more suitable representation than in linear elasticity of rubber elasticity.

This second approach is then chosen on account of requiring less challenging arithmetic operations. Using Equation 3.5 and the chain rule, one is able to derive Equation 3.4 in t, the pseudotime, and finally obtain the large strains equivalent of Equation 2.7, gathered in Table 6[2].

Apart from that, finding the *critical time* becomes also more complicated. In this case, a more elaborated iterative scheme is required to solve the non-linear equation that allows to find t_c such that Equation 3.4 holds for $x^*(t_c) = 0$:

$$\int_0^L \sqrt{1 - 2e(x, t_c)}\, dx = L. \tag{3.6}$$

2 If $e \ll 1$, then the ODEs shown tend to the ones presented in Table 3.

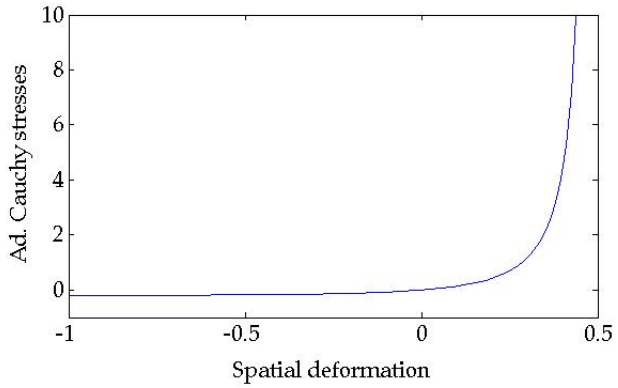

Figure 17: Spatial St.Venant-Kirchhoff constitutive relation.

On the other hand, a similar idea is applied at the location problem to compute $\hat{t}$. In this case, the non-linear equation for the correct $\hat{t}$ reads

$$x^* \sqrt{1-2\alpha} + \int_{x^*}^{L} \sqrt{1-2e(x)}\, dx = L. \tag{3.7}$$

Remind that these strategies consider a St.Venant-Kirchoff hyperelastic material. It is not on the scope of this thesis to discuss the most suitable hyperelastic model for inextensibility problems, but to qualitatively assess the increased difficulty of dealing with them with respect to a linear framework.

Furthermore, observation of Figure 17 evidences the poor representativity of this model for elastomers, because such materials are expected to strecth far more than the maximum 50% allowed for a St.Venant-Kirchhoff material.

3.3 NUMERICAL EXAMPLES

Numerical implementation of the above described algorithms follows the same ideas described in Chapter 2. Let us give now an example that combines both localization and evolution strategies in a hyperelastic setting.

A 1D truss with an extensibility limit $\alpha = 0.05$ subject to an external load of $b(x,t) = (0.4 - 0.02t);\ 0 \leqslant x \leqslant 1,\ t \in [0,10]$ is considered. In this case the focus is not put on modeling the progressive application of a load, but simply a variable external load.

If $x_0 = 0.3$ is the initial approximation, then at $t = 0$ a locating scheme is required to find the correct position of the

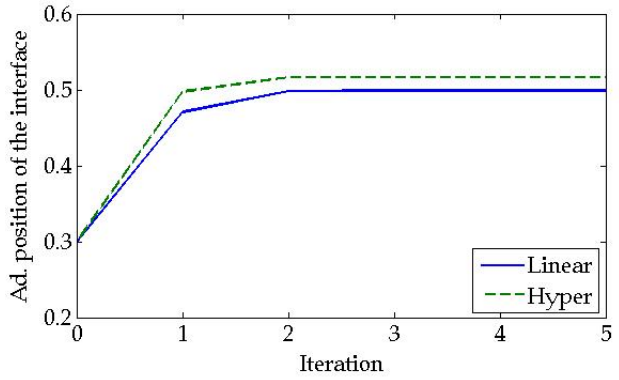

(a) Evolution of the interface within the location scheme.

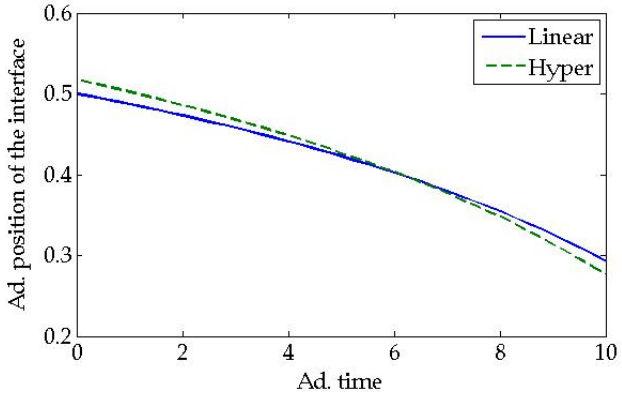

(b) Evolution of the interface due to change in external load.

Figure 18: Tracking the interface with a St.V-K. model.

interface. After that, one continues migrating the interface up to $t = 10$ with an evolving scheme. Figure 18 displays the numerical results and shows the discrepancy with linear elasticity.

Analysis of this example and observation of the written algorithms and ODEs allows to conclude that locating and evolving the interface is essentially the same idea, a relevant outcome of this study.

The sensitivity of the interface, that is, how it does move, is the same for both cases, the only difference between the methods is the cause of migration and, more precisely, the cause of non-equilibrium.

When locating the interface, the displacement of the interface is due to the incorrect position of the interface, whereas in evolution problems, the interface displaces as a consequence of a variation in the external load.

Finally, Figure 19 depicts the evolution of the interface for another two-interface problem. In this case, $\alpha = 0.05$ and $b(x, t) = 0.2(1.5 - x)$.

Compared with Figure 15, the sense of migration of the interfaces is reversed and simmetry is lost due to the change in the boundary condition. The corresponding terms of the associated DAEs are given in Table 7.

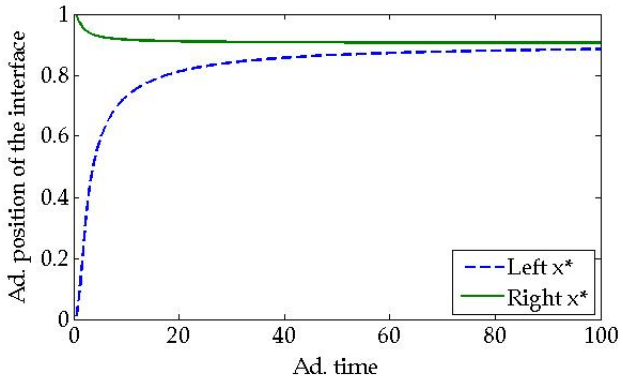

Figure 19: Two-interface case in hyperelasticity.

	DIRICHLET B.C. - SPATIAL DESCRIPTION
$M(t, \mathbf{x}^*)$	$\beta(t) \int_{x^-}^{x^+} \frac{(1-2e(x,t))^2}{1+e(x,t)} dx \begin{pmatrix} b_0(x^+(t)) & 0 \\ 0 & b_0(x^-(t)) \end{pmatrix}$
$\mathbf{f}(t, \mathbf{x}^*)$	$\dot{\beta}(t) \begin{pmatrix} \int_{x^-}^{x^+} \frac{(1-2e(x,t))^2}{1+e(x,t)} \left(\int_{x^+}^{x} b_0(s) ds \right) dx \\ \int_{x^-}^{x^+} \frac{(1-2e(x,t))^2}{1+e(x,t)} \left(\int_{x^-}^{x} b_0(s) ds \right) dx \end{pmatrix}$

Table 7: Terms in Equation 2.10 associated to the solution in Figure 19.

In this case, the evolution of the interfaces is not independent of each other, that is, a coupled scheme is obtained. Therefore, for a Dirichlet case, nature of the problem determines whether the DAEs system is coupled or decoupled.

4

EXTENSION OF THE 1D METHODS TO HIGHER DIMENSIONS

Explicit methods to locate and evolve the interface in 1D linear elastic problems have been devised in Chapter 2. Adaptation of these methods to a 1D large strains scenario has been dealt in Chapter 3. An expansion to 2D or 3D problems is proposed in this chapter to conclude the study.

It is clear that higher dimensions introduce extra complexity into the inextensibility model. Aspects such as modeling the interface, moving it accordingly and numerical simulation of the nonlinear kinematics are not as straightforward as earlier and require more sophisticated techniques presented in Section 4.1.

After that, Section 4.2 provides a possible way to locate and evolve the interface in 2D or 3D hyperelasticity. No numerical experiments are carried out, since they are deemed outside of the scope of this thesis.

4.1 ADDITIONAL MODELING TOOLS

4.1.1 *X-FEM and Level set methods*

The interface in multidimensional problems is a more complex entity than a point, namely, a curve in 2D or a surface in 3D. As seen in Section 1.2.1, along the interface the strain field is discontinuous.

If a standard FEM is employed, then the interface must be meshed, which is not convenient in problems involving location and evolution processes.

For instance, possible large distortions of the mesh could arise from the interface motion and impose frequent remeshing operations.

Aimed at avoiding to mesh the discontinuity while keeping the robustness of the FEM, the *eXtended Finite Element Method*

(XFEM), Möes et al. [11], has been designed and widely employed to model and propagate discontinuities in many physical problems.

The X-FEM approach uses the partition of unity, Melenk and Babuška [10] and Babuška and Melenk [1], to define a suitable local enrichment of the finite element space.

In this manner, a representation of a discontinuity in a field is obtained, without affecting the sparsity of the stiffness matrix, see Figure 20.

Apart from that, the basic framework for capturing the geometry of a moving boundary or interface is the notion of Level set.

Introduced by Osher and Sethian [14] the *Level set method* translates the geometry of the discontinuity into numerics and allows for its propagation by means of robust algorithms.

Assignment of a signed distance function to an implicit manifold is quite a simple task. Using this idea, it is possible to represent the geometry of a discontinuity as the zero iso-contour of a scalar function ϕ defined over Ω, see Figure 21.

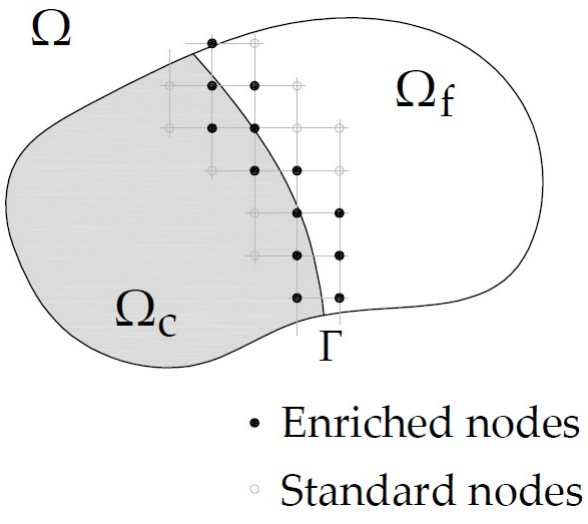

Figure 20: X-FEM enrichment strategy close to the interface.

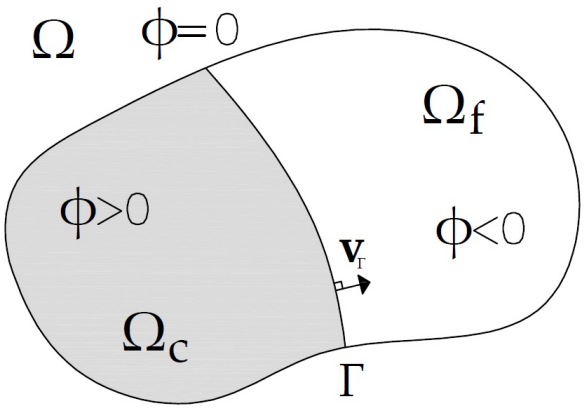

Figure 21: Level set function over Ω.

Function ϕ is the so called Level set function and the zero iso-contour, that is, the description of Γ is obtained by interpolation on the mesh.

In terms of evolution, for a particle on the interface it is required that

$$\varphi(\mathbf{x}(t), t) = 0. \tag{4.1}$$

If $\mathbf{v}_\Gamma$ denotes the outward normal velocity of the interface, then the chain rule yields the fundamental Level set equation

$$\phi_t + \mathbf{v}_\Gamma \cdot \nabla\phi = 0, \tag{4.2}$$

also called the Hamilton-Jacobi equation, which acts as the governing equation of the interface evolution.

Osher and Sethian [14] devise algorithms to numerically propagate the interface using Equation 4.2. Note that this method naturally adapts to topological changes, see Figure 22, and is thought from an Eulerian perspective.

By coupling the X-FEM with a Level-set method, one obtains a numerical technique to treat mechanical problems involving moving boundaries and interfaces.

4.1.2 *Shape sensitivity analysis*

Sensitivity of the solution to an incorrectly located interface or a change in the external load was directly assessed via derivation of the equilibrium equation in 1D problems; indeed, the

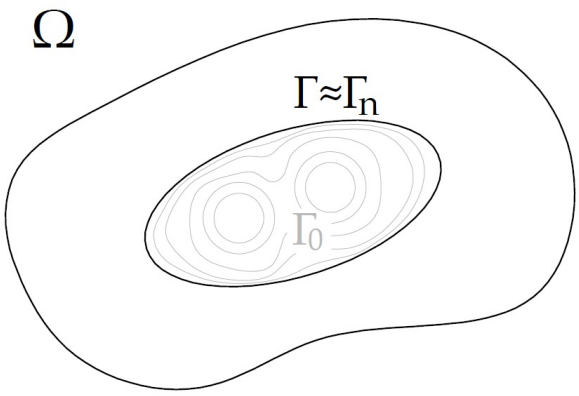

Figure 22: Natural changes in topology of the Level set. Adapted from Bonfils et al. [3].

interface point $x^*(t)$ could be treated as a variable and it made sense to find $\dot{x}^*(t)$.

This is no longer available in a 2D or 3D scenario, where the solution is obtained from minimization of the total potential energy. For these cases, the sensitivity analysis can be performed using the concept of *shape derivative*, Taroco [17].

To introduce this technique, it is convenient to reinterpret the problem: A domain with a moving boundary or interface can also be understood as a domain undergoing a shape variation process.

Hence, let us identifiy the initial shape of the body with Ω. The shape change of Ω can be characterized by the transformation

$$\mathbf{x}^\tau = \mathbf{x} + \tau\mathbf{v}(\mathbf{x}), \tag{4.3}$$

see describing Figure 23, where $\mathbf{v}(\mathbf{x})$ is a known, sufficiently smooth vector field and τ is a scalar parameter. Here $\mathbf{x}$ identifies the initial coordinates.

Addition of superscript τ marks the dependence of the transformation on this parameter and also denotes the transformed coordinates $\mathbf{x}^\tau$ and the transformed domain Ω^τ.

At each τ the shape change is a one-to-one correspondence between Ω and Ω^τ. As a result of this, any scalar function, vec-

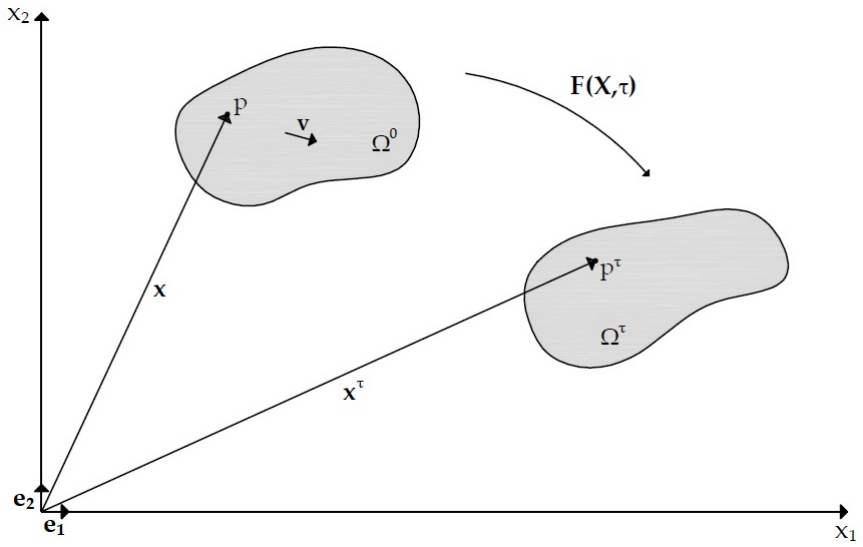

Figure 23: Shape transformation in 2D.

tor or tensor field can be defined either in Ω or in Ω^τ.

More interestingly, an analogy with the continuum mechanics framework can be established, where the initial shape corresponds to the material description and the transformed shape to the spatial description.

That means it is possible to assimilate the change of shape to the motion of a body; indeed, $\mathbf{v}$ acts as the velocity field associated to the motion and the equivalent form of the deformation gradient tensor, the change of shape gradient tensor, reads

$$\mathbf{F} = \nabla \left[\mathbf{x} + \tau\mathbf{v}(\mathbf{x})\right] = \mathbf{Id} + \tau\nabla\mathbf{v}. \tag{4.4}$$

As detailed in [17], the shape derivative of the total potential energy, that is, the sensitivity of the solution to the motion of the interface is obtained by an analogous application of the Gâteaux derivative, see Oliver and Agelet [13].

4.1.3 *Arbitrary Lagrangian-Eulerian methods*

The choice of a kinematical description of the continuum should adapt to the nature of the inextensibility problem. Furthermore, this decision will determine the relationship between the finite element space and the deformed continuum.

Two classical approaches arise from the two main descriptions of motion in continuum mechanics: In Lagrangian algorithms, each node follows an associated particle during motion, whereas in Eulerian algorithms the continuum moves with respect to a fixed computational mesh.

Where the first group risks of showing mesh regularity issues following large distorsions of the continuum, the second is subject to poorly accurate representations of the moving boundary or interface.

In an attempt to combine the advantages of both families of algorithms, while minimizing its weaknesses, the *Arbitrary Lagrangian-Eulerian methods* have been devised, Donea et al. [5].

The main feature of these methods consists in the ability of freely moving the computational mesh. This will be useful when tracking the interface, as it will be seen in Section 4.2.

ALE methods are based on a generalization of the classical Lagrangian and Eulerian descriptions of motion. In the ALE kinematical description, the points of the grid at each t are identified with reference coordinates $\boldsymbol{\chi}$ belonging to the referential configuration Ω_R^t.

The referential configuration Ω_R^t is neither the material nor the spatial configurations. Figure 24 depicts these three domains and the one-to-one correspondences linking them. Note that the particle motion $\boldsymbol{\varphi}$ is then expressed as

$$\boldsymbol{\varphi} = \boldsymbol{\Phi} \circ \boldsymbol{\Psi}^{-1}. \tag{4.5}$$

According to this framework, the material and the mesh move with respect to the laboratory with different velocities. In particular, the relative velocity between the material and the mesh, alternatively called the convective velocity $\mathbf{c}$, is defined as

$$\mathbf{c} := \mathbf{v} - \hat{\mathbf{v}} = \frac{\partial \mathbf{x}}{\partial \boldsymbol{\chi}} \cdot \mathbf{w}, \tag{4.6}$$

where $\mathbf{v}$ is the material velocity, $\hat{\mathbf{v}}$ the mesh velocity and $\mathbf{w}$ the particle velocity as seen from the referential domain. It is clear that both Lagrangian or Eulerian formulations may be obtained as particular cases, depending on the choice of $\boldsymbol{\Psi}$ or $\boldsymbol{\Phi}$.

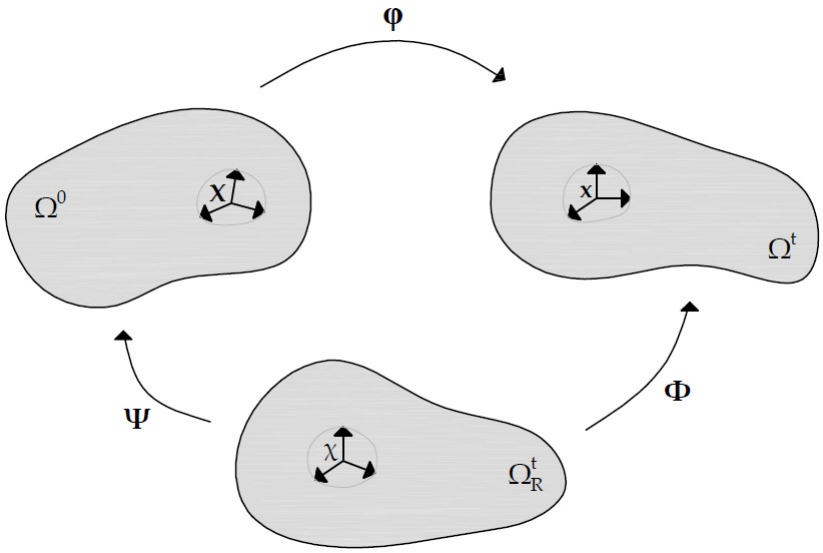

Figure 24: Transformations between referential and classical configurations. Adapted from Donea et al. [5].

Furthermore, the relation between the material time derivative and the referential time derivative is given by the so called ALE fundamental equation, that is,

$$\left.\frac{\partial f}{\partial t}\right|_{\mathbf{x}} = \left.\frac{\partial f}{\partial t}\right|_{\boldsymbol{\chi}} + \mathbf{c}\cdot\nabla f. \tag{4.7}$$

If f is a physical quantity, then Equation 4.7 shows that the material derivative is its local (referential) derivative plus a convective term taking into account the relative motion between the material and the referential systems.[1]

As detailed in [5], the conservation laws for mass, momentum and energy in ALE framework are expressed in terms of the referential time derivative using Equation 4.7. These equations are then used as the basis for the spatial discretization of the problem.

By specifying a mesh velocity $\hat{\mathbf{v}}$ that conforms to the problem under consideration, one can avoid large distortions of the mesh, while preserving an acceptable accuracy in the representation of the moving boundary or interface.

1 As in Eulerian algorithms, ALE methods are not free of convective effects, but freedom in the choice of mesh velocity allows to reduce the numerical issues associated to the convective nonsymmetric operators.

4.2 A PROPOSAL OF EXTENSION

Let us now describe a way to extend the preceding 1D analysis to multidimensional problems. For this purpose, the same ideas developed so far will be invoked, but they will be adapted with the modeling tools introduced in Section 4.1.

After observing the front evolution algorithm provided in Bonfils et al. [3] it is concluded that the Newton-Raphson iterative scheme designed in Section 2.2, see Equation 2.4 and Table 2, is a particular case of the latter.

In order to propagate the interface, one needs first to project the equilibrium solution and find its sensitivity on the interface. After that, the application of the Newton-Raphson method in a finite element framework leads to solve a linear system that gives the velocity of the interface $\mathbf{v}_\Gamma$.

It is relevant to point out that the volumetric kinematical constraint allows to assume that $\mathbf{v}_\Gamma$ is normal to the interface. Therefore, it is only needed to obtain its modulus at each propagation step.

In a large strains framework, the equilibrium solution could arise from an ALE variational form of the problem, solved by means of an X-FEM/Level set coupled strategy. This would give the residual tension on the interface.

Apart from that, the sensitivity of the solution would be evaluated only in a neighbourhhood of the interface, as it is not needed anywhere else, using the notion of shape derivative.

After evaluating the velocity of the interface $\mathbf{v}_\Gamma$, it would be required to propagate the Level set, that is, the application of Equation 4.2, if a classical approach was used.

Nonetheless, the flexibility of the ALE spares us this update, provided $\hat{\mathbf{v}} = \mathbf{v}_\Gamma$ on Γ at each step. This is, in fact, the motivation behind the choice of an ALE kinematical description for large strains inextensibility models.

Figure 25 indicates a possible specification for the mesh or grid velocity $\hat{\mathbf{v}}$ with an ALE method. In this case, the nodes on

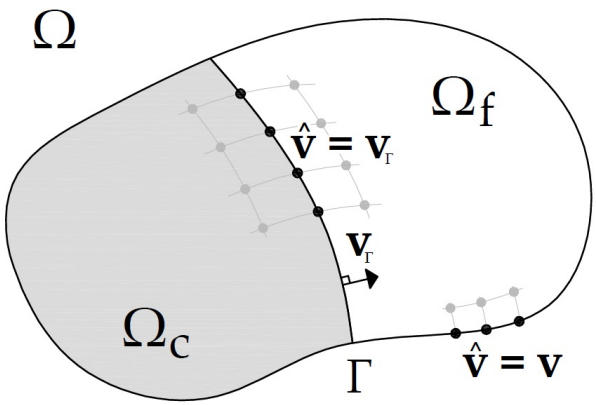

Figure 25: Proposed way to move the mesh with an ALE method.

the interface Γ move at $\mathbf{v}_\Gamma$, whereas the nodes on the free boundary move according to the deformation of the continuum.

An appropriate interpolation strategy would complete the definition of the velocity field on the grid. Note that careful discretization would be required as to avoid decompensation issues, such as an exceedingly coarse mesh at either the constrained or the free finite spaces.

In contrast with [3], the method does not adapt naturally to topological changes. That means, for instance, starting an iterative scheme with an incorrect topology of the interface will not lead to the solution unlesh remeshing is done.

In spite of the drawbacks, the strategy devised here is very attractive, because the ALE method does not only better conform to the deformation of the continuum than a classical approach, but makes it easier to propage its interface.

5

CONCLUSIONS AND SUMMARY OF RESULTS

Many applications in civil engineering involve the use of elastomers. Although these materials admit large deformations, they have a limit on its extensibility. Therefore, numerical modeling of these materials only makes sense in a large strains framework.

Treatment of inextensibility constraints in hyperelastic materials involves two sources of nonlinearity: the constraint in the constitutive model and the kinematics of the finite strain framework.

In 1D linear elasticity, the latter source does not apply. As a consequence of this, iterative schemes to locate and evolve one or multiple interfaces have been easily obtained and they are characterized by its explicitness.

The extension to a simple 1D large strains scenario, that is, incorporation of the nonlinear kinematics, has highlighted the increase in complexity of the problem. Even though the developed algorithms can be rewritten, they are no longer as direct, explicit and versatile as before.

Numerical examples have shown that location and evolution of the interface can be understood as the same problem, with the exception of the driving effect; indeed, the cause of non-equilibrium for a location scheme is the incorrect position of the interface, whereas a change in the external load stands for the cause in evolution schemes.

Finally, an extension to a multidimensional framework has been designed. The same ideas in the 1D analysis can be applied with the help of additional modeling tools: the X-FEM and Level set methods, the shape sensitivity analysis and the Arbitrary Lagrangian-Eulerian methods.

According to the proposed approach, a stepwise update of the Level set would be unnecessary, which is an important com-

putational benefit regarding the interface propagation.

Further development of this MSc thesis shall numerically test this method and confirm its computational advantages. Apart from that, the strategies introduced here may also be relevant to other engineering problems with interfaces, such as plasticity analysis or the saturation of a porous medium.

Part II

APPENDIX

A

VARIATIONAL FORM IN 2D LINEAR ELASTICITY

As a natural extension of Section 1.2.1, the variational formulation of Table 1 is detailed in this appendix.

Let us first introduce the strain energy functions in Ω_c and Ω_f:

$$\psi_c = \tfrac{1}{2}\,\boldsymbol{\varepsilon} : \mathbb{C} : \boldsymbol{\varepsilon} + \chi_A \qquad \psi_f = \tfrac{1}{2}\,\boldsymbol{\varepsilon} : \mathbb{C} : \boldsymbol{\varepsilon}, \tag{A.1}$$

where χ_A is the characteristic function of the subset $A \subset \Omega$ given by

$$A = \{\mathbf{x} \in \Omega : \mathrm{tr}\boldsymbol{\varepsilon}(\mathbf{x}) - \alpha = 0\}. \tag{A.2}$$

Then, the total potential energy $\mathcal{U}(\mathbf{u})$ of the system is written as

$$\mathcal{U}(\mathbf{u}) = \int_{\Omega_c} \psi_c(\boldsymbol{\varepsilon})\mathrm{d}\Omega + \int_{\Omega_f} \psi_f(\boldsymbol{\varepsilon})\mathrm{d}\Omega - \int_{\Omega} \mathbf{b}\cdot\mathbf{u}\mathrm{d}\Omega - \int_{\Gamma_n} \mathbf{t_n}\cdot\mathbf{u}\mathrm{d}\Omega. \tag{A.3}$$

The minimization of the above functional yields the variational form or weak form of the problem:

find $(\mathbf{u}, p)$ such that:

$$\begin{aligned} a(\mathbf{u},\mathbf{v}) + b(\mathbf{v},p) &= \mathcal{F}(\mathbf{v}) \quad \text{for all } \mathbf{v} \text{ in } V^0 \\ b(\mathbf{u},q) &= \mathcal{G}(q) \quad \text{for all } q \text{ in } L^2(\Omega), \end{aligned} \tag{A.4}$$

where the above functionals read

$$\begin{aligned} a(\mathbf{u},\mathbf{v}) &= \int_{\Omega} \boldsymbol{\varepsilon}(\mathbf{u}) : \mathbb{C} : \boldsymbol{\varepsilon}(\mathbf{v})\mathrm{d}\Omega, \\ b(\mathbf{u},p) &= \int_{\Omega_c} p\,\mathrm{tr}\boldsymbol{\varepsilon}(\mathbf{u})\mathrm{d}\Omega, \\ \mathcal{F}(\mathbf{u}) &= \int_{\Omega} \mathbf{b}\cdot\mathbf{u}\mathrm{d}\Omega + \int_{\Gamma_n} \mathbf{t_n}\cdot\mathbf{u}\mathrm{d}\Omega, \\ \mathcal{G}(p) &= \int_{\Omega_c} \alpha p\mathrm{d}\Omega, \end{aligned} \tag{A.5}$$

and the space of kinematically admissible spaces is defined as

$$\begin{aligned} V &= \{\mathbf{v} \in H^1(\Omega) : \mathbf{v} = \mathbf{u}_d \text{ on } \Gamma_d\}, \\ V^0 &= \{\mathbf{v} \in H^1(\Omega) : \mathbf{v} = \mathbf{0} \text{ on } \Gamma_d\}. \end{aligned} \tag{A.6}$$

B

ANALYTICAL SOLUTION IN 1D LINEAR ELASTICITY

The analytical solution of a 1D linear elastic bar fixed at its left edge with an extensibility limit and subject to a prescribed load reads

$$p(x) = \begin{cases} \int_x^L b(s)ds - E\alpha & \text{if } 0 \leqslant x \leqslant x^* \\ 0 & \text{if } x^* < x \leqslant L, \end{cases} \tag{B.1}$$

$$\varepsilon(x) = \begin{cases} \alpha & \text{if } 0 \leqslant x \leqslant x^* \\ \frac{1}{E}\int_x^L b(s)ds & \text{if } x^* < x \leqslant L, \end{cases} \tag{B.2}$$

$$u(x) = \begin{cases} \alpha x & \text{if } 0 \leqslant x \leqslant x^* \\ \alpha x^* + \frac{1}{E}\int_{x^*}^x \left(\int_t^L b(s)ds\right) dt & \text{if } x^* < x \leqslant L. \end{cases} \tag{B.3}$$

Moreover, for x^*

$$\alpha = \frac{1}{E}\int_{x^*}^L b(s)ds \tag{B.4}$$

holds.

Finally, the Lagrange multiplier admits to be interpreted as

$$p(x) = \langle \sigma(x) - E\alpha \rangle. \tag{B.5}$$

C

EVOLUTION OF THE INTERFACE IN 1D LINEAR ELASTICITY

Let us develop the procedure of obtention of the interface evolving schemes presented in Section 2.3.

C.1 NEUMANN CASE:

Assume first a Neumann boundary condition at the tip of the 1D truss, that is,

$$\sigma(L,t) \equiv \hat{t} \quad \forall t > 0. \tag{C.1}$$

By writing the equilibrium equation in $[x^*(t), L]$,

$$\hat{t} = \sigma(L,t) = E\alpha - \beta(t)c_0(x^*(t)), \tag{C.2}$$

and derivating in time,

$$\begin{aligned} 0 &= \frac{d}{dt}\{E\alpha - \beta(t)c_0(x^*(t))\} \\ &= -\dot{\beta}(t)c_0(x^*(t)) + \beta(t)b_0(x^*(t))\dot{x}^*(t), \end{aligned} \tag{C.3}$$

one gets straightforwardly at the expression provided in Table 3.

C.2 DIRICHLET CASE:

Suppose now a Dirichlet boundary condition at the tip of the 1D truss, such as

$$u(L,t) \equiv \hat{u} \quad \forall t > 0. \tag{C.4}$$

Let us first write the Cauchy equation and the Lagrange multiplier:

$$\sigma(x,t) = \sigma(L,t) + \int_x^L b(s,t)ds \tag{C.5}$$

$$p(x,t) = \langle \sigma(x,t) - E\alpha \rangle. \tag{C.6}$$

By using the constitutive relation $\varepsilon(x,t) = \sigma(x,t) - p(x,t)$, one gets

$$\varepsilon(x,t) = \begin{cases} \alpha & \text{if } x \in [0, x^*(t)] \\ \frac{\sigma(x,t)}{E} & \text{if } x \in (x^*(t), L], \end{cases} \tag{C.7}$$

where the position of the interface $x^* \in [0, L]$ is assumed known.

On the other hand, the geometric equation (compatibility condition) allows relating the prescribed displacement with the prescribed load and position of the interface:

$$\begin{aligned} \hat{u} &= \int_0^L \varepsilon(s,t)ds \\ &= \int_0^{x^*(t)} \alpha ds + \int_{x^*(t)}^L \frac{\sigma(s,t)}{E} ds \\ &= \alpha x^*(t) + (L - x^*(t)) \frac{\sigma(L,t)}{E} + \frac{1}{E} \int_{x^*(t)}^L \left(\int_s^L b(x,q)dq \right) ds \\ &= \alpha x^*(t) + (L - x^*(t)) \frac{\sigma(L,t)}{E} + \frac{1}{E} \int_{x^*(t)}^L \left(\beta(t) \int_s^L b_0(q)dq \right) ds \\ &= \alpha x^*(t) + (L - x^*(t)) \frac{\sigma(L,t)}{E} + \frac{\beta(t)}{E} \int_{x^*(t)}^L \left(\int_s^L b_0(q)dq \right) ds. \end{aligned} \tag{C.8}$$

Introducing

$$c_0(x) := \int_x^L b_0(s)ds \tag{C.9}$$

and imposing equilibrium at $x^*(t)$ yields

$$\sigma(L,t) = E\alpha - \beta(t)\int_{x^*(t)}^{L} b_0(s)ds. \tag{C.10}$$

Thus, an expression whose only unknown is the function $x^*(t)$ is obtained, that is,

$$\hat{u} = \alpha L + \frac{\beta(t)}{E}\left[\int_{x^*(t)}^{L} [c_0(s) - (L - x^*(t))b_0(s)]\, ds\right]. \tag{C.11}$$

Derivation of the previous expression gives finally a relation between the velocity of the interface and the evolution of the prescribed load and displacement:

$$\begin{aligned}
0 &= \frac{\dot{\beta}(t)}{E}\left[\int_{x^*(t)}^{L} [c_0(s) - (L - x^*(t))b_0(s)]\, ds\right] \\
&\quad + \frac{\beta(t)}{E}\frac{d}{dt}\left\{\int_{x^*(t)}^{L} [c_0(s) - (L - x^*(t))b_0(s)]\, ds\right\} \\
&= \frac{\dot{\beta}(t)}{E}\left[\int_{x^*(t)}^{L} [c_0(s) - (L - x^*(t))b_0(s)]\, ds\right] \\
&\quad + \frac{\beta(t)}{E}\frac{d}{dt}\left[-c_0(x^*(t)) + \int_{x^*(t)}^{L} b_0(s)ds + (L - x^*(t))b_0(x^*(t))\right] \\
&= \frac{1}{E}\left[\int_{x^*(t)}^{L} [c_0(s) - (L - x^*(t))b_0(s)]\, ds\right] \cdot \dot{\beta}(t) \\
&\quad + \frac{\beta(t)}{E}(L - x^*(t))b_0(x^*(t)) \cdot \dot{x}^*(t)
\end{aligned} \tag{C.12}$$

The above expression can be easily reinterpreted as the ODE provided in Table 3, if one proceeds analogously, but imposing the equilibrium in $[x^*(t), x]$ instead of $[x^*(t), L]$.

D

THE CONCEPT OF CRITICAL TIME APPLIED TO A SIMPLE CASE

In order to provide a better understanding of the *critical time*, suppose first a 1D linear elastic bar fixed at its left edge subject to a constant steady load $b_0(x) \equiv b,\ b \in [E\alpha, \infty)$ with a linear time factor $\beta(t) = t,\ \forall t \in [0, \infty)$.

A few calculations give that

$$\begin{aligned} x^*(t) &= L - \frac{E\alpha}{b_0 t} \Rightarrow t_c = \frac{E\alpha}{b_0 L}, \\ \dot{x}^*(t) &= \frac{E\alpha}{b_0}\frac{1}{t^2} \Rightarrow \dot{x}^*(t_c) = \frac{b_0 L^2}{E\alpha}. \end{aligned} \tag{D.1}$$

Let us now change the Neumann b.c. (bar fixed at its left edge) for an homogeneous Dirichlet b.c. (bar fixed at both edges). In this case, one gets

$$\begin{aligned} x^*(t) &= \sqrt{L^2 - \frac{2E\alpha L}{b_0 t}} \Rightarrow t_c = \frac{2E\alpha}{b_0 L}, \\ \dot{x}^*(t) &= \frac{E\alpha L}{b_0 t^2}\left(L^2 - \frac{2E\alpha L}{b_0 t}\right)^{-\frac{1}{2}} \Rightarrow \lim_{t \to t_c^+} \dot{x}^*(t) = \infty. \end{aligned} \tag{D.2}$$

That means a singularity appears precisely at the critical time, see Figure 26. Since $\dot{x}^*(t_c) = 0$ holds, one can numerically integrate the solution without evaluating the function at t_c recurring to a fully implicit method such as the backward Euler, as it is appointed in Section 2.4.1.

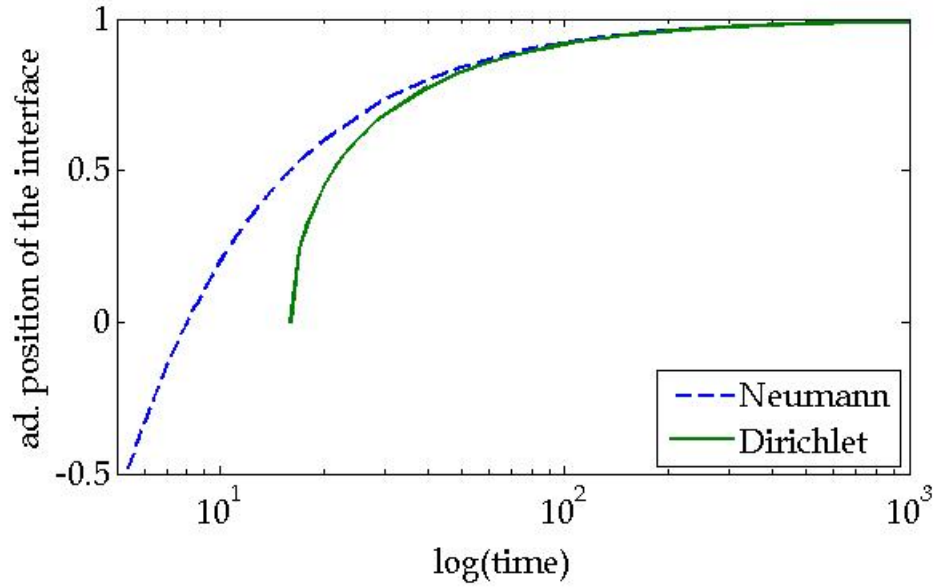

Figure 26: Critical time and position of the interface, $\frac{E\alpha}{b_0} = 8$.

E

NUMERICAL SOLUTION IN 1D ST.VENANT-KIRCHHOFF HYPERELASTICITY

This appendix provides two possible ways to numerically evaluate the position of the interface in a 1D truss modeled as a St.Venant-Kirchhoff material.

Basic hypothesis comply with the ones given in Chapter 3. Additionally, a Neumann boundary condition is prescribed at the tip of the 1D truss (bar fixed at its left edge) and the solution is obtained in the Eulerian or spatial description.

The strong form associated to the problem when no extensibility limit applies is given in Table 8.

Introduction of the constitutive relation into the equilibrium equation and addition of the Lagrange multiplier p allows to write the ODE associated to the inextensibility model:

$$\begin{aligned} \tfrac{dp}{dx} + b(x) &= 0 \qquad x \in [0, x^*], \\ g(\tfrac{du}{dx})\tfrac{d^2u}{dx^2} + b(x) &= 0 \quad x \in (x^*, L], \end{aligned} \tag{E.1}$$

where function g reads

$$g\left(\frac{du}{dx}\right) = \left(1 - \frac{du}{dx}\right)\frac{1 + e(x)}{(1 - 2e(x))^{(5/2)}}. \tag{E.2}$$

Mechanical equilibrium	$\frac{d\sigma}{dx} + b(x) = 0$
Constitutive relation	$\sigma(x) = \frac{2\mu e(x)}{(1-2e(x)^{(3/2)}}$
Kinematic condition	$e(x) = \frac{du}{dx} - \frac{1}{2}\left(\frac{du}{dx}\right)^2$
Boundary conditions	$u(0) = 0$
	$\sigma(1) = 0$

Table 8: Strong form of the spatial 1D St.Venant-Kirchhoff model.

E.1 COUPLED METHOD

According to this method, the position of the interface results from solving the non-linear equation

$$\text{find } x^* \in [0, L] \text{ s. t. } \sigma(x = 1; x^*) = 0, \tag{E.3}$$

where the evaluation of the objective function follows these two steps, given $x^* \in [0, 1]$,

1. solve in the constrained domain the BVP (shooting method):

$$\frac{d\mathbf{u_1}}{dx} = \mathbf{b}(x, \mathbf{u_1}), \quad x \in [0, x^*] \tag{E.4}$$

$$\mathbf{u_1} = \begin{Bmatrix} u(x) \\ \frac{du}{dx} \\ p(x) \end{Bmatrix}, \quad \mathbf{b}(x, \mathbf{u_1}) = \begin{Bmatrix} u_{12} \\ 0 \\ -b(x) \end{Bmatrix}, \quad \begin{Bmatrix} u_{11}(0) = 0 \\ u_{12}(x^*) = 1 - \sqrt{1 - 2\alpha} \\ u_{13}(x^*) = 0 \end{Bmatrix}.$$

2. Then solve in the free domain the IVP:

$$\frac{d\mathbf{u_2}}{dx} = \mathbf{b}(x, \mathbf{u_2}), \quad x \in (x^*, L] \tag{E.5}$$

$$\mathbf{u_2} = \begin{Bmatrix} u(x) \\ \frac{du}{dx} \\ p(x) \end{Bmatrix}, \quad \mathbf{b}(x, \mathbf{u_2}) = \begin{Bmatrix} u_{22} \\ -\frac{b(x)}{g(u_{22})} \\ 0 \end{Bmatrix}, \quad \mathbf{u_2}(x^*) = \mathbf{u_1}(x^*).$$

E.2 DECOUPLED METHOD

Let us remark that the decomposed problem in $(x^*, L]$ is a full Neumann BVP.

Therefore, it must be first found x^* such that equilibrium in $(x^*, L]$ holds, which corresponds to solve the problem:

$$\text{find } x^* \in [0, L] \text{ s. t. } 2\mu \frac{\alpha}{(1 - 2\alpha)^{(3/2)}} - \int_{x^*}^{L} b(x)dx = 0. \tag{E.6}$$

After that, one possibility to obtain the solution is by integrating first the BVP in $[0, x^*]$ and then the IVP in $(x^*, L]$ as shown in the previous point. Some modifications allow to reverse the order of integration.

E.3 ANALYSIS

Let us conclude this appendix with some brief remarks and conclusions regarding the two methods described:

- If $\alpha \ll 1$, then

$$e(x) \leqslant \alpha \Leftrightarrow \frac{du}{dx} \leqslant 1 - \sqrt{1-2\alpha} \approx \alpha + O(\alpha^2), \qquad \text{(E.7)}$$

  which means that either the small strains and the St.Venant-Kirchhoff models provide similar solutions.

- The *coupled* scheme provides the solution of the problem together with $[0, x^*]$, in contrast with the *decoupled scheme*.

- Both alternatives involve solving iterative schemes: one for $[0, x^*]$ and another for the BVP in $[0, x^*]$. The *coupled* scheme embeds one scheme into the other, whereas the *decoupled* scheme solves them separately. Therefore, the *coupled* method is computationally more convenient.

BIBLIOGRAPHY

[1] I. Babuška and J. Melenk. Partition of unity method. *International Journal for Numerical Methods in Engineering*, 40(4): 727–758, 1997.

[2] J. Bonet and R.D. Wood. *Hyperelasticity*. Cambridge University Press, Cambridge, second edition, 2008. ISBN 0-521-57272-X.

[3] N. Bonfils, N. Chevaugeon, and N. Möes. Treating volumetric inequality constraint in a continuum media with a coupled x-fem/level-set strategy. *Computer Methods in Applied Mechanics and Engineering*, 205-208:16–28, 2012.

[4] J.M.G. Cowie. *Polymers: chemistry and physics of modern materials*. Nelson Thornes Ltd, Glasgow, second edition, 1991. ISBN 0-7487-4073-2.

[5] J. Donea, A. Huerta, J.-Ph. Ponthot, and A. Rodríguez-Ferran. Arbitrarian Lagrangian-Eulerian Methods. In E. Stein, R. De Borst, and T.J.R. Hughes, editors, *Encyclopedia Of Computational Mechanics.*, volume 1, chapter 14, pages 413–437. John Wiley and Sons, Ltd., Chichester, England, 2004. ISBN 978-0-470-84699-5.

[6] J.R. Dormand and P.J. Prince. A family of embedded Runge-Kutta formulae. *Journal of Computational and Applied Mathematics*, 6:19–26, 1980.

[7] A.N. Gent. Extensibility of rubber under different types of deformation. *Journal of Rheology*, 49(1):271–275, 2005.

[8] E. Hairer and G. Wanner. *Solving Ordinary Differential Equations II: Stiff and Differential-Algebraic Problems*. Springer-Verlag, Berlin, second edition, 1996. ISBN 9783540604525.

[9] J.D. Lambert. *Numerical methods for ordinary differential systems: the initial value problem*. John Wiley and Sons, Ltd., Chichester, England, 1991. ISBN 0471929905.

[10] J. Melenk and I. Babuška. The partition of unity finite element method: Basic theory and applications. *Computer*

Methods in Applied Mechanics and Engineering, 39:289–314, 1996.

[11] N. Möes, J. Dolbow, and T. Belytschko. A finite element method for crack growth without remeshing. *International Journal of Numerical Methods in Engineering*, 46:131–150, 1999.

[12] J. Nocedal and S.J. Wright. Theory of constrained optimization. In *Numerical Optimization*, chapter 12, pages 314–359. Springer-Verlag, New York, first edition, 1999. ISBN 0-387-98793-2.

[13] X. Oliver and C. Agelet. *Mecánica de medios continuos para ingenieros*. Edicions UPC, Barcelona, second edition, 2002. ISBN 978-84-8301-582-7.

[14] S. Osher and J. A. Sethian. Fronts propagating with curvature-dependent speed: Algorithms based on Hamilton-Jacobi formulations. *Journal of Computational Physics*, 79(1):12–49, 1988.

[15] A. Quarteroni. *Numerical models for differential problems*. Springer-Verlag, Milano, 2009. ISBN 9788847010710.

[16] M. Spivak. *Calculus on Manifolds*. Westview Press, Boulder, USA, fifth edition, 1971. ISBN 9780805390216.

[17] E. Taroco. Shape sensitivity analysis in linear elastic fracture mechanics. *Computer Methods in Applied Mechanics and Engineering*, 188:697–712, 2000.